Journal of Electrostatics 103 (2020) 103406

Contents lists available at ScienceDirect

Journal of Electrostatics

journal homepage: http://www.elsevier.com/locate/elstat

Improved control over polymer nanofiber deposition with a programmable 3-axis electrospinning apparatus

Maximilian Sonntag [a], Amanda Cimino [a], Maheshinie Rajapaksha [b], Joanna Thomas [a,*]

[a] Biomedical Engineering, Mercer University School of Engineering, Macon, GA, USA
[b] Biomedical Sciences, Mercer University School of Medicine, Macon, GA, USA

ARTICLE INFO

Keywords:
Electrospinning
Nanofibers
CAD-Controlled
G-code

ABSTRACT

We built an electrospinning apparatus that integrates conventional electrospinning components with an FDM 3D-printing configuration, including real-time 3-axis control to improve accuracy and precision in nanofiber deposition over conventional far-field electrospinning. We motion-synced the spinneret needle and ground needle, incorporated a silver-coated stabilizer on the spinneret needle, and placed an aluminum-surfaced disc on the ground needle. Tests were executed to optimize accurate and precise, dry nanofiber collection at a typical flow rate and applied voltages. Our computer-controlled prototype maintained typical nanofiber characteristics obtained with far-field electrospinning while demonstrating it is capable of accurate stationary deposition and dynamic geometric patterning.

1. Introduction

A typical electrospinning apparatus generates dense, macroscopically 2D sheets of nanofiber material [1–3]. Most require an electrically grounded collecting surface, a liquid polymer-solvent mixture in a syringe, a voltage source (≤50 kV) and a syringe pump. A positive charge is applied to the polymer-solvent mixture as it is pumped through a needle. With the appropriate flow rate and applied voltage, the solvent evaporates as the polymer jet is drawn into a thin fiber between the needle and a grounded collecting surface. This process inherently lacks precision beyond one's ability to control the nanofiber alignment and nanofiber ultrastructure via polymer chemistry, polymer-solvent combinations, and collector conformations [4–7]. Improved control over fiber deposition, without transitioning to a direct-write or near-field electrospinning system [8,9], could enable more rapid generation of tailored 2D constructs, possibly even 3D constructs for a variety of applications while maintaining the nanofiber ultrastructure achieved with traditional electrospinning.

In light of this, we have built a unique electrospinning apparatus utilizing 3D printing technologies and common electrospinning equipment. In our apparatus, we implemented a silver-coated spinneret stabilizer, a motion-synced spinneret needle and ground needle, an aluminum-surfaced ground disc, and precise automated control over needle-to-collector distance (Z_o). We evaluated the effects of these design features and capabilities on fiber deposition diameter and center-point deviation as well as fiber characteristics. In addition, we executed two dynamic utility tests to demonstrate the level of control achieved over the nanofiber deposition pattern.

2. Materials and methods

2.1. Electrospinning apparatus

Our electrospinning apparatus (3DE) consists of two vertically aligned needles – an extruding spinneret needle (spinneret, Fig. 1, part 3) and a ground needle (ground, Fig. 1, part 6). The two needles are attached to carriages (Fig. 1-A and Fig. 1-B) that move along the x-axis in synchrony to keep the needles aligned at all times. The 23 Ga stainless steel spinneret needle (Hamilton, USA) was connected via PTFE tubing (Fig. 1A, part 1) to a syringe pump NE-4000 (New Era Pump Systems, Inc., USA) and via an insulated cable (Fig. 1A, part 2) to a voltage source (Gamma High Voltage Research, ES30P–10W, USA). We also fabricated a disc-shaped, silver-coated stabilizer that attached to the end of the spinneret with a 2 mm offset from the tip (Fig. 1-A, part 4). Lastly, a ground disc (Fig. 1-B, part 5), covered with an aluminum sheet on the top surface was attached flush with the tip of the ground. A porous alumina silicate ceramic plate (McMaster-Carr USA, 9″ x 9″ x 1/8″) served as the collector between the spinneret and the ground (Fig. 1,

* Corresponding author. 1501 Mercer University Drive, Macon, GA, 31207, USA.
E-mail address: Thomas_JL@mercer.edu (J. Thomas).

https://doi.org/10.1016/j.elstat.2019.103406
Received 13 September 2019; Received in revised form 8 November 2019; Accepted 19 November 2019
Available online 31 December 2019

part 9); the collector plate was suspended over the ground and moved along the y-axis. The precise spinneret tip to collector plate distance, z-offset (Z_o), was controlled via programmed movement of the spinneret carriage along the z-axis. Movement along all axes (x, y, and z) was controlled by pairs of Nema17 stepper motors. The system was driven by computer numerical control (CNC) through a modified version of Marlin (v1.1) that interprets standard G-code.

2.2. Polymer solution preparation

A 10% w/v polycaprolactone (PCL; Sigma-Aldrich, average M_n 80,000) solution in Chloroform/N,N-Dimethylformaldehyde (7:3) was stirred for 24 h and used within the following 24 h at room temperature (~22 °C).

2.3. Parameter optimization

Stationary spot tests were performed to identify optimal Z_o for accurate fiber deposition with and without the spinneret stabilizer. All tests were conducted with an applied voltage of 10 kV–15 kV, a flow rate of 0.5 ml/h, and a ground disc diameter (G_d) of 6.8 mm–7.8 mm. The synced spinneret and ground were positioned, via G-code, at each spot for 60 s (n = 9). Z_o was increased at 10 mm increments from 30 mm–60 mm. Image analysis to determine deposition diameter and the center-point deviation was done in Photoshop. Statistical significance ($p < 0.05$) was determined by unpaired *t*-test.

2.4. Transmission electron microscopy (TEM)

For the parameters that yielded the smallest spot test diameters, fiber samples were collected on carbon-coated copper grids for 30 s (n = 3 grids). Images were taken on a JEM 2100 Plus TEM (JEOL Ltd., Tokyo, Japan) at 80 kV and 6 K magnification equipped with a 4 K Oneview CMOS CCD camera (15 images per condition). Fiber diameters were measured using ImageJ (n = 150). Statistical significance ($p < 0.05$) was determined by unpaired *t*-test.

2.5. Utility tests

Dynamic tests were performed with the stabilizer, ground disc of 6.8 mm–7.8 mm, a flow rate of 0.5 ml/h, and an applied voltage of 15 kV to assess the capacity of the 3DE to generate simple shapes. In the first test conducted, the 3DE was programed to 'print' an 8 cm straight line. To confirm that 60 mm was the optimal Z_o with the stabilizer, Z_o was incrementally increased for each test from 40 mm to 70 mm (n = 6 per Z_o). The G-code for this test was generated using Simplify3D. Images of the test outcomes were taken with an iPhone 7, and the width of the lines were measured in Photoshop.

In the second test, the 3DE was tasked to 'print' a square (5 cm × 5 cm) composed of 5 uniform outlines with a line width of 10 mm and 50% overlap (n = 3 per Z_o); the G-code dictated that the 3DE would trace the square pattern twice, essentially laying down two layers. The CAD model was generated in SolidWorks and exported as a STL file. The STL file was imported into Simplify3D in which a custom profile had been created for the 3DE. Key parameters used included: scan speed = 1 mm/s, extrusion width = 10 mm, primary layer height = 50 μm, outlines = 100% (forcing only outlines and no infill pattern), outline overlap = 50%, and horizontal size compensation = −5 mm. The program generated a preview of the path that the needle pair would trace for each layer and then exported it as G-code for the controller of the 3DE. Again, Z_o was incrementally increased for each test, this time 45 mm–65 mm (n = 3 per Z_o). All electrospinning parameters were maintained from the line test. Images of the test outcomes were taken with an iPhone 7, and the squares were evaluated against the modeled pattern in Photoshop.

3. Results & discussion

Although electrospinning is not a new technique, alternative arrangements of the traditional configuration and the introduction of new components continue to broaden its applications and utility [10–15]. Our aim was to preserve dry deposition of <500 nm fiber diameters, which have been shown to promote cell adhesion in scaffolds for tissue enginnering [16,17], while improving control over fiber deposition. Mats of aligned nanofiber scaffolds have been readily fabricated [6, 18–20], but patterning the nanofiber deposition with traditional electrospinning has proven more difficult [21]. Melt electrospinning and direct write electrospinning offer greater control but generally yield larger fiber diameters or slower output, respectively [9,22]. Considering demand for scale-up in scaffold fabrication, we targeted improving control while maintaining the yield of traditional electrospinning and other techniques for nanofiber production such as pressurized gyration.

Finite element analysis (FEA) indicates the impacts of the spinneret

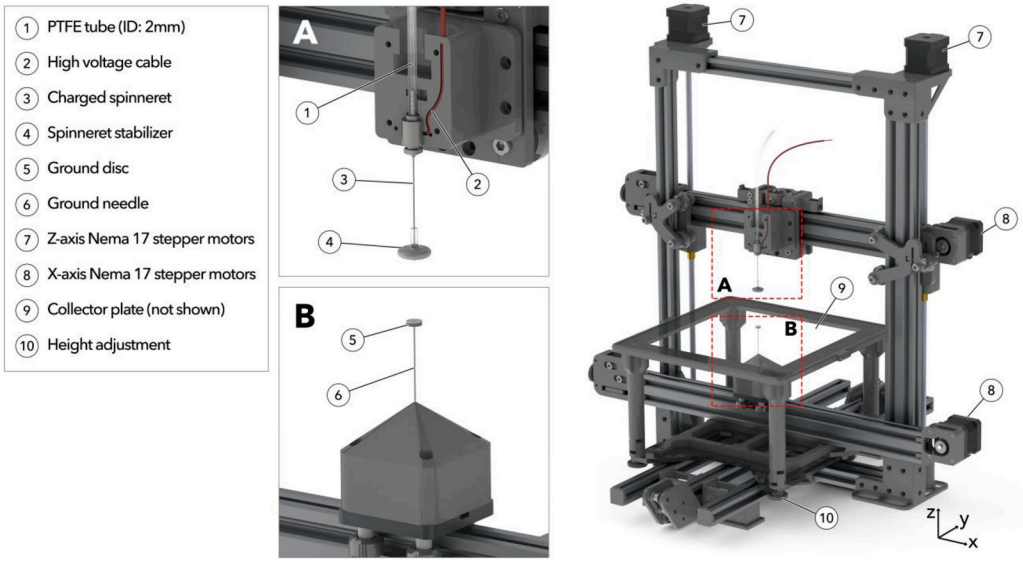

Fig. 1. 3DE design and components. The 3-axis system controls spinneret position in relation to the ceramic collector (not shown). (A) Spinneret electric field is modified via a silver-coated stabilizer, Part 4. (B) Spinneret motion in x-direction is synced with a ground needle, Part 6. An aluminum-surfaced ground disc is attached to the tip of the needle, Part 5.

stabilizer we incorporated on the electric field (e-field) are strongest near the spinneret tip and stabilizer (Fig. S1); we propose the e-field lines proximal to the spinneret tip and Taylor cone hold the fiber in a straight flight path farther than a conventional electrospinning set up. At the midpoint between the spinneret and the ground, FEA simulations show that the e-field strength drops (Figs. S1–C). Studies show that the decrease in the e-field influence allows enough instability for fibers to oscillate or whip, resulting in fiber thinning [23]. Subsequently, with an optimal Z_o, the solvent fully evaporates from the fibers and the fibers achieve the desired nanoscale dimensions prior to entering the focusing e-field of the ground disc and ground needle (Figs. S1–D).

3.1. Parameter optimization

Stationary spot tests were performed as a first step to determine the effects of the spinneret stabilizer and identify an optimal Z_o (Fig. 2). Due to the color and porous nature of our collector plate, wet deposition was readily evident at the macroscopic level (Supp. Video 1 & Fig. S2). Overall, spot diameter is reduced by decreasing Z_o, and we found significant correlations between Z_o and spot diameter (Fig. S3, A-C). With the stabilizer, deposition at $Z_o < 50$ mm was wet; thus, those parameters were not considered adequate to generate dry nanofibers, and measurements were excluded from consideration for optimal parameters. The smallest dry deposition diameter we observed, 12.24 ± 0.89 mm, was at a Z_o of 30 mm without the stabilizer (Fig. 2A). At a Z_o of 60 mm, with the stabilizer, we saw a dry deposition diameter of 12.67 ± 1.63 mm (Fig. 2B); these spot diameter results were not significantly different than the results without the stabilizer (Fig. 2C) demonstrating the stabilizer is not necessary to achieve precise results. However, our center-point deviation results indicate that the stabilizer significantly improves the accuracy of the fiber deposition. Center-point deviation with the stabilizer, 3.33 ± 0.41 mm, was less than half the center-point deviation seen without the stabilizer, 7.65 ± 1.27 mm (Fig. 2D, $p < 0.01$). Hence, the stabilizer significantly improved deposition accuracy while maintaining precision.

3.2. Nanofiber characteristics

Representative images of the nanofibers generated with and without stabilizer are shown in Fig. 3A and B. Nanofibers were qualitatively consistent in shape and distribution across all samples. With the stabilizer and $Z_o = 60$ mm, the fiber diameters were 120.8 ± 3.33 nm; without the stabilizer and $Z_o = 30$ mm, the fiber diameters were significantly thicker at 152.5 ± 4.49 nm ($p < 0.01$, $n = 150$) (Fig. 3C). This difference is in large part due to the greater range of fiber thicknesses seen in samples generated without the stabilizer (49.8 nm–295.7 nm with stabilizer vs 49.9 nm–475.4 nm without stabilizer). Potentially, without the stabilizer, the electric field is more susceptible to fluctuations, resulting in less consistent effects on fiber thinning.

3.3. Utility tests

For the line test (Fig. 4A & B), the Z_o was varied from 40 to 70 mm to confirm that a Z_o of 60 mm yielded the most accurate result; specifically, that the fiber deposition was 8 cm long and 10 mm wide. We observed wet or mixed deposition at $Z_o \leq 55$ mm. Fig. 4A shows the transition from wet deposition to dry deposition, left to right. Note that when deposition is wet the polymer appears opaque and amorphous. As Z_o was increased the additional distance traveled by the polymer jet provided time for the solvent to nearly fully evaporate (Supp V1 vs Supp V2). The increase in Z_o also allowed for more whipping and subsequent widening of the flight path of the fiber. The density of dry fiber deposition is greatest along the center of the line, a phenomenon previously observed in other studies [9,24]; the contrast between the white polymer fibers and the grey ceramic collector produces an ombré effect from the center of the line towards the edges that is more noticeable at $Z_o \geq 60$ mm. Thus, as anticipated, the width of fiber deposition increased from 4.31 ± 0.30 mm to 18.70 ± 1.19 mm as Z_o was increased. The line length and deposition width matched the Simplify 3D simulation at a Z_o of 60 mm (line width $= 9.48 \pm 0.41$ mm).

Based on the line test findings, we predicted a more complex 2D shape could be generated in a manner similar to fused deposition manufacturing. Via the software, the 3DE can be programmed to print multiple layers, so we generated a G-code file to output a pattern of nanofibers within a 5 cm × 5 cm square (Fig. 4C). Two layers were printed with a 50% overlap for the path in each layer to improve uniformity. Optimal geometric control with dry deposition was achieved at a Z_o of 60 mm which supports the results seen with the line test.

Similar to our findings from the spot tests, the solvent failed to fully evaporate at 40 mm (Supp V1) and 45 mm; the partially wet deposition appears to cause fiber cohesion resulting in a mixture of solid polymer masses and nanofibers. At Z_o of 60 mm the fiber deposition was accurate (Supp V2); the 'printed' square has identifiable corners, nearly uniform coverage, and is cleanly within the programmed design perimeter shown in red. No visible deflection or repulsion of the second layer is evident so we anticipate that printing multi-layered structures is feasible without loss of accuracy. Beyond Z_o of 60 mm we saw good coverage within the square; however, the corners and edges began to lose definition.

At a line speed of 1 mm/s the 3DE completes two layers of deposition covering an area of 25 cm^2 in 30 s; thus, it could achieve 50 layers in

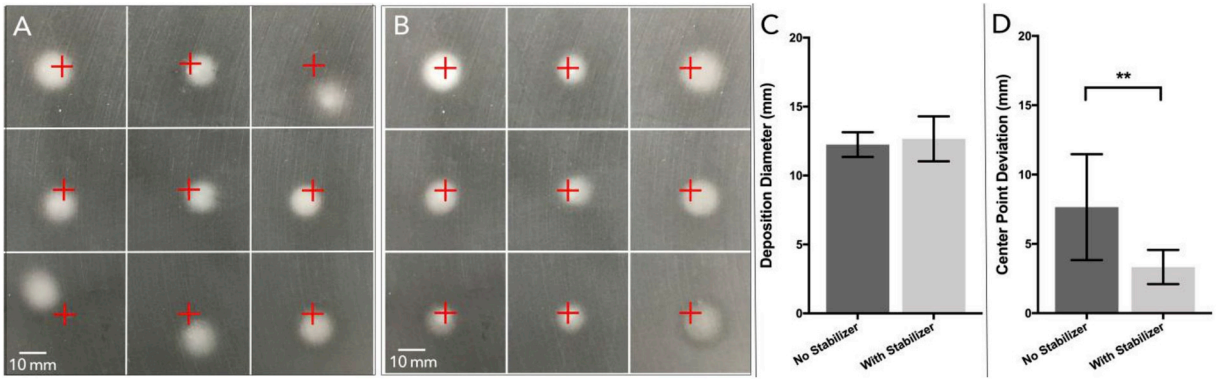

Fig. 2. Spinneret stabilizer improves fiber deposition control. Spinneret was held stationary directly above marked locations (red crosses) for 60 s. **A)** Smallest spot test results without stabilizer were at $Z_o = 30$ mm, **B)** Smallest spot test results with stabilizer were at $Z_o = 60$ mm, **C)** Smallest spot diameter was not different with or without spinneret stabilizer (12.67 ± 1.63 mm vs. 12.24 ± 0.89 mm, error bars = SD), **D)** Spot deposition was more accurate, i.e. center point deviation was significantly smaller with the stabilizer (3.33 ± 0.41 mm vs 7.65 ± 1.27 mm, $^{**}p < 0.01$, error bars = SD). (For interpretation of the references to color in this figure legend, the reader is referred to the Web version of this article.)

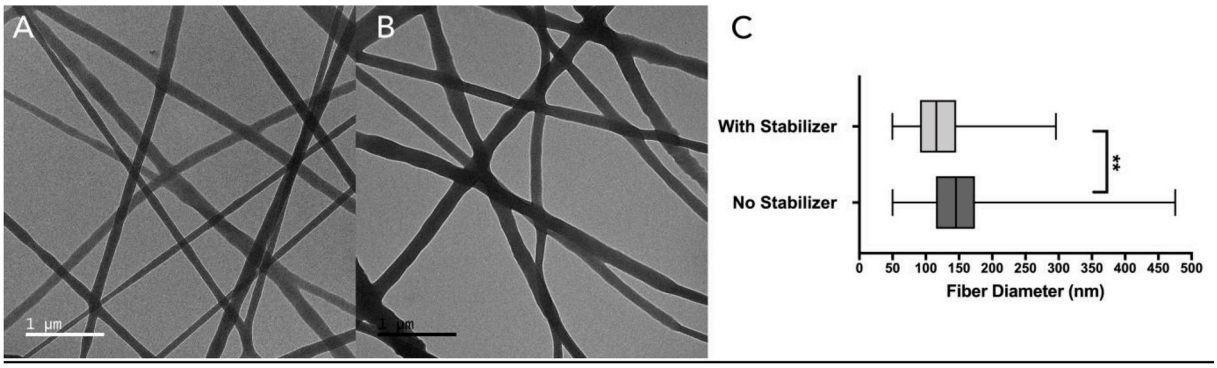

Fig. 3. Nanofiber characteristics. A) Nanofibers collected with the spinneret stabilizer at $Z_o = 60$ mm and 15 kV. **B)** Nanofibers collected without the spinneret stabilizer at $Z_o = 30$ mm and 10 kV. **C)** Nanofiber diameters were significantly thinner with a smaller range of thicknesses with the spinneret stabilizer (120.8 ± 3.33 nm vs. 152.5 ± 4.49 nm, **p < 0.01), error bars show min/max fiber diameter (n = 150).

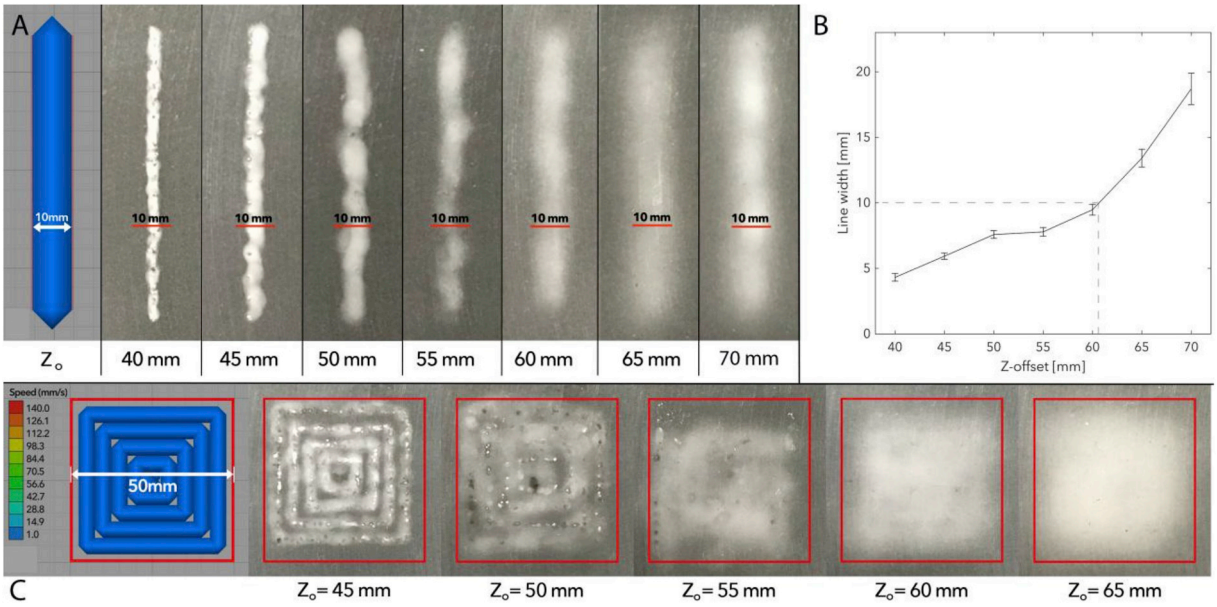

Fig. 4. Utility tests of 3DE. A) Line width test. The simulated G-code is programmed to a line width of 10 mm. The test was conducted with Z_o from 40 to 70 mm in 5 mm increments, **B)** The line width generated by the 3DE matches the simulation at $Z_o = 60$ mm, **C)** Two-layer square test was performed at Z_o from 45 to 65 mm in 5 mm increments.

<15 min (estimated layer thickness of 750 nm). Other direct write electrospinning systems or electrohydrodynamic (EHD) systems are estimated to take in excess of 30 h [9] or 3 h [15] to generate a 37.5 μm × 5 cm x 5 cm square. Melt electrospinning methods with flow rates often below 100 μl/h would take even longer [24]. Although the 3DE potentially has a >10-fold reduction in fabrication time over an EHD system, the scaffolds generated by the 3DE and an EHD are distinctly different. The 3DE output is a randomly aligned mat of nanofibers, each under 400 nm in diameter. EHD fibers are generally >5 μm in diameter, so a 'solid' 37.5 μm 5 cm × 5 cm square would require several layers of aligned fibers. Porosity can be tightly controlled with the EHD system; a porous sample would also reduce fabrication time. Alternatively, while cells can migrate through micron scale pores and attach to >1 μm diameter fibers, collagen fibrils and other fibrilar protein that comprise the extracellular matrix (ECM) range in diameter from 5 nm to 500 nm. So, the 3DE output could be considered more ECM-like for tissue engineering applications.

The 3DE parameter configurations detailed in this work yield accurate patterns of nanofibers on a macroscopic scale. The 3DE lines, 10 mm wide, were comprised of randomly deposited nanofibers ranging from 50 nm–300 nm in diameter. Other studies utilizing near-field electrospinning have fabricated similarly dimensioned nanofibers and demonstrated nanoscale level control [9,13]. While it was not our intent to for the 3DE to operate as a near-field electrospinning apparatus, it should be noted that we expect it is capable of operation with parameters similar to near-field electrospinning systems. Near-field systems utilize much lower applied voltages (200 V–500 V), faster line speeds (5 mm/s – 40 mm/s) and shorter Z_o (1 mm–5 mm) to fabricate patterns and figures with single fibers in the nano-to micrometer range. The highly controlled deposition of single fibers also requires reduced polymer flow rates (0.5–400 μl/h). We speculate that the 3DE's stabilizer and the motion-synced spinneret and ground, coupled with a smaller gauge spinneret could provide nanoscale control at near-field electrospinning parameters utilizing higher polymer flow rates. As another option, the 3DE could be retrofitted as a coaxial EHD system. It currently utilizes a single spinneret needle with an inner diameter of ~337 μm. A new carriage for the 3DE could be 3D printed to accommodate an alternative spinneret, additional tubing, and any necessary wiring. The standard applied voltage (1 kV–15 kV) and line speed (40 mm/s to 150 mm/s) for EHD systems are within the operational bounds as well for the 3DE. An electrospinning system with this level of adaptability via minor changes to accessible components and computer-controlled parameter

adjustments would be a valuable asset in a research lab as well as a useful tool in teaching electrostatics.

4. Conclusion

In summary, our results demonstrate the components of the 3DE: 1) significantly reduce center-point deviation for more accurate fiber deposition, 2) maintain the typical nanofiber ultrastructure seen with conventional far-field electrospinning, and 3) readily generate layered nanofiber mats in basic 2D patterns and shapes. These initial studies show that the 3DE in its current configuration has potential to be a versatile apparatus for fabricating macroscopic patterns of randomly aligned polymer nanofiber mats as well as multi-layered polymer nanofiber structures. Future experiments are planned to confirm that the combination of the e-field generated by the spinneret stabilizer, and the ground disc, are responsible for the improved precision and accuracy in fiber deposition control as observed with the 3DE. We will also conduct additional SEM studies to characterize the yield and multi-layer morphology of the 3DE output. While much work remains to determine the 3DE's full capacity, we are excited by our preliminary findings and plan to continue to investigate the extent of the 3DE's versatility.

Declaration of conflicting interest

The authors declare no potential conflicts of interest with respect to the research, authorship, and/or publication of this article.

Acknowledgments

The authors would like to thank Dorina Mihut for her help and expertise in material sputter coating. This project was supported by a Mercer University QEP Award and a Mercer University Seed Grant; no persons, other than the authors, contributed to study design, data collection and analysis, and manuscript preparation.

Appendix A. Supplementary data

Supplementary data to this article can be found online at https://doi.org/10.1016/j.elstat.2019.103406.

References

[1] A. Formhals, US Patent US2323025A, 1943.
[2] G. Taylor, Electrically driven jets, Proc. R. Soc. A Math. Phys. Eng. Sci. 313 (1969) 453–475, https://doi.org/10.1098/rspa.1969.0205.
[3] M. Goldberg, R. Langer, X. Jia, Nanostructured materials for applications in drug delivery and tissue engineering, J. Biomater. Sci. Polym. Ed. 18 (2007) 241–268, https://doi.org/10.1163/156856207779996931.
[4] T.J. Sill, H.A. von Recum, Electrospinning: applications in drug delivery and tissue engineering, Biomaterials 29 (2008) 1989–2006, https://doi.org/10.1016/j.biomaterials.2008.01.011.
[5] M.K. Leach, Z.-Q. Feng, S.J. Tuck, J.M. Corey, Electrospinning fundamentals: optimizing solution and apparatus parameters, J. Vis. Exp. 2494 (2011), https://doi.org/10.3791/2494.
[6] P.L. Heseltine, J. Ahmed, M. Edirisinghe, Developments in pressurized gyration for the mass production of polymeric fibers, Macromol. Mater. Eng. 303 (2018) 1800218, https://doi.org/10.1002/mame.201800218.
[7] W. Hwang, C. Pang, H. Chae, Fabrication of aligned nanofibers by electric-field-controlled electrospinning: insulating-block method, Nanotechnology 27 (2016) 435301, https://doi.org/10.1088/0957-4484/27/43/435301.
[8] G. Luo, K.S. Teh, Y. Liu, X. Zang, Z. Wen, L. Lin, Direct-write, self-aligned electrospinning on paper for controllable fabrication of three-dimensional structures, ACS Appl. Mater. Interfaces 7 (2015) 27765–27770, https://doi.org/10.1021/acsami.5b08909.
[9] H. Chen, A. de B.F.B. Malheiro, C. van Blitterswijk, C. Mota, P.A. Wieringa, L. Moroni, Direct writing electrospinning of scaffolds with multidimensional fiber architecture for hierarchical tissue engineering, ACS Appl. Mater. Interfaces 9 (2017) 38187–38200, https://doi.org/10.1021/acsami.7b07151.
[10] W.-E. Teo, R. Inai, S. Ramakrishna, Technological advances in electrospinning of nanofibers, Sci. Technol. Adv. Mater. 12 (2011), 013002, https://doi.org/10.1088/1468-6996/12/1/11660944.
[11] G. Bisht, S. Nesterenko, L. Kulinsky, M. Madou, A computer-controlled near-field electrospinning setup and its graphic user interface for precision patterning of functional nanofibers on 2D and 3D substrates, J. Lab. Autom. 17 (2012) 302–308, https://doi.org/10.1177/2211068212446372.
[12] G.S. Bisht, G. Canton, A. Mirsepassi, L. Kulinsky, S. Oh, D. Dunn-Rankin, M. J. Madou, Controlled continuous patterning of polymeric nanofibers on three-dimensional substrates using low-voltage near-field electrospinning, Nano Lett. 11 (2011) 1831–1837, https://doi.org/10.1021/nl2006164.
[13] J. Lee, S.Y. Lee, J. Jang, Y.H. Jeong, D.-W. Cho, Fabrication of patterned nanofibrous mats using direct-write electrospinning, Langmuir 28 (2012) 7267–7275, https://doi.org/10.1021/la3009249.
[14] S. Labbaf, H. Ghanbar, E. Stride, M. Edirisinghe, Macromol. Rapid commun. 6/2014, Macromol. Rapid Commun. 35 (2014), https://doi.org/10.1002/marc.201470019, 593–593.
[15] D. Wang, X. Zhao, Y. Lin, T. Ren, J. Liang, C. Liu, L. Wang, Fabrication of micro/nano- structures by electrohydrodynamic jet technique, Front. Mech. Eng. 12 (2017) 477–489, https://doi.org/10.1007/s11465-017-0461-y.
[16] J.L. Lowery, N. Datta, G.C. Rutledge, Effect of fiber diameter, pore size and seeding method on growth of human dermal fibroblasts in electrospun poly (ϵ-caprolactone) fibrous mats, Biomaterials 31 (2010) 491–504, https://doi.org/10.1016/j.biomaterials.2009.09.072.
[17] S.H. Ku, S.H. Lee, C.B. Park, Synergic effects of nanofiber alignment and electroactivity on myoblast differentiation, Biomaterials 33 (2012) 6098–6104, https://doi.org/10.1016/j.biomaterials.2012.05.018.
[18] F. Yang, R. Murugan, S. Wang, S. Ramakrishna, Electrospinning of nano/micro scale poly(l- lactic acid) aligned fibers and their potential in neural tissue engineering, Biomaterials 26 (2005) 2603–2610, https://doi.org/10.1016/j.biomaterials.2004.06.051.
[19] C.E. Ayres, G.L. Bowlin, R. Pizinger, L.T. Taylor, C.A. Keen, D.G. Simpson, Incremental changes in anisotropy induce incremental changes in the material properties of electrospun scaffolds, Acta Biomater. 3 (2007) 651–661, https://doi.org/10.1016/j.actbio.2007.02.010.
[20] H. Cao, K. Mchugh, S.Y. Chew, J.M. Anderson, The topographical effect of electrospun nanofibrous scaffolds on the *in vivo* and *in vitro* foreign body reaction, J. Biomed. Mater. Res. 9999A (2009), https://doi.org/10.1002/jbm.a.32609. NA-NA.
[21] D. Li, G. Ouyang, J.T. McCann, Y. Xia, Collecting electrospun nanofibers with patterned electrodes, Nano Lett. 5 (2005) 913–916, https://doi.org/10.1021/nl0504235.
[22] P.D. Dalton, Melt electrowriting with additive manufacturing principles, Curr. Opin. Biomed. Eng. 2 (2017) 49–57, https://doi.org/10.1016/j.cobme.2017.05.007.
[23] A.H. Nurfaizey, J. Stanger, N. Tucker, N. Buunk, A.R. Wood, M.P. Staiger, Control of spatial deposition of electrospun fiber using electric field manipulation, J. Eng. Fibers. Fabrics 9 (2014), https://doi.org/10.1177/155892501400900118, 155892501400900.
[24] P.D. Dalton, N.T. Joergensen, J. Groll, M. Moeller, Patterned melt electrospun substrates for tissue engineering, Biomed. Mater. 3 (2008), 034109, https://doi.org/10.1088/1748-6041/3/3/034109.